OPEN ACCESS
IOP Publishing
Plasma Physics and Controlled Fusion
Plasma Phys. Control. Fusion **61** (2019) 034001 (9pp)
https://doi.org/10.1088/1361-6587/aaf596

Bremsstrahlung emission profile from intense laser-solid interactions as a function of laser focal spot size

C D Armstrong[1,2], C M Brenner[2], E Zemaityte[1,2], G G Scott[2], D R Rusby[2], G Liao[3], H Liu[2,4], Y Li[4], Z Zhang[4], Y Zhang[2,4], B Zhu[4], P Bradford[5], N C Woolsey[5], P Oliveira[2], C Spindloe[2], W Wang[4], P McKenna[1] and D Neely[2]

[1] Department of Physics SUPA, University of Strathclyde, Glasgow G4 0NG, United Kingdom
[2] Central Laser Facility, STFC Rutherford Appleton Laboratory, Harwell, OXON, OX11 0QX, United Kingdom
[3] Key Laboratory for Laser Plasmas (Ministry of Education) and School of Physics and Astronomy, Shanghai Jiao Tong University, Shanghai 200240, People's Republic of China
[4] Beijing National Laboratory for Condensed Matter Physics, Institute of Physics, Chinese Academy of Sciences, Beijing 100190, People's Republic of China
[5] Department of Physics, York Plasma Institute, University of York, Heslington York YO10 5DD, United Kingdom

E-mail: chris.armstrong@stfc.ac.uk

Received 30 August 2018, revised 13 November 2018
Accepted for publication 3 December 2018
Published 23 January 2019

Abstract

The bremsstrahlung x-ray emission profile from high intensity laser-solid interactions provides valuable insight to the internal fast electron transport. Using penumbral imaging, we characterise the spatial profile of this bremsstrahlung source as a function of laser intensity by incrementally increasing the laser focal spot size on target. The experimental data shows a dual-source structure; one from the central channel of electrons, the second a larger substrate source from the recirculating electron current. The results demonstrate than an order of magnitude improvement in the intensity contrast between the two x-ray sources is achieved with a large focal spot, indicating preferable conditions for applications in radiography. An analytical model is derived to describe the transport of suprathermal electron populations that contribute to substrate and central channel sources through a target. The model is in good agreement with the experimental results presented here and furthermore is applied to predict laser intensities for achieving optimum spatial contrast for a variety of target materials and thicknesses.

Keywords: bremsstrahlung, penumbral, laser-plasma, defocus, x-ray source size, x-ray radiography

(Some figures may appear in colour only in the online journal)

1. Introduction

High intensity laser pulses rapidly ionise the target material and accelerate electrons in laser-solid interactions, driving a multi-MegaAmpere current of relativistic electrons into the target [1–3]. This electron current collisionally causes further ionisation within the target leading to characteristic line emission, and produces broad-band bremsstrahlung radiation

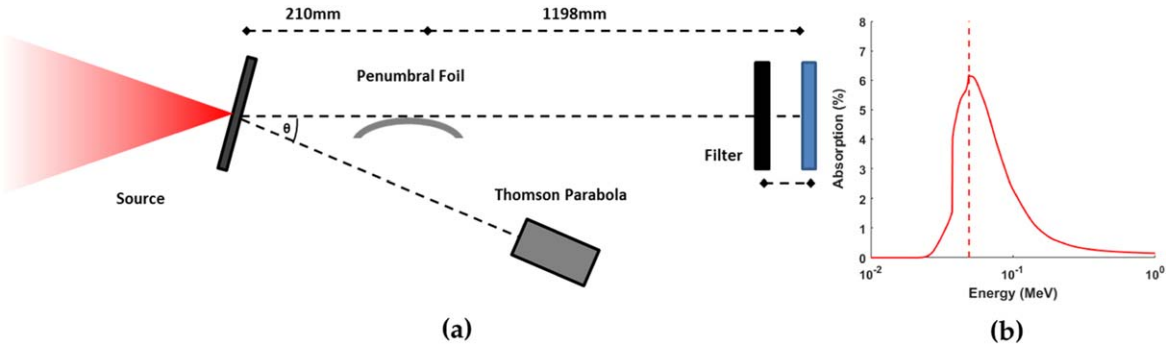

Figure 1. (a) Top view of the experimental layout, showing the distances to the penumbral foil and detector stack, and the positioning of the Thomson parabola. θ is 15°, denoting the angle from laser axis. Between the detector and the source is an 18 mm SiO_2 filter. (b) Response curve of penumbral image plate in the detector. Dashed line highlights critical x-ray energy, ∼50 keV.

with energies up to tens of MeV as it propagates [4, 5]. This emission of bremsstrahlung radiation has long been used as a high energy x-ray source for radiography [6, 7]. Both bremsstrahlung and line emission are used as a diagnostic tool for laser-plasma interactions [8–12]. To optimise the x-ray brightness while minimising the source size it is necessary to understand the generation and transport of the electron beam as it propagates through the target. In doing so, we can improve the performance of these sources for x-ray radiography applications.

The incident laser pulse drives an electron beam with some initial divergence into the target. This divergence is, in part, due to intensity variation in the laser focal spot profile [13]. As the fast electrons travel through the target, an azimuthal magnetic field is established that acts to confine the electron beam, higher current density increases the strength of the magnetic field [14, 15]. This effect is particularly present in thick (>300 μm) targets where higher accelerated proton energies than a simple ballistic electron expansion model predicted were detected as a result of the magnetic field growth limiting the electron expansion [16]. As electrons reach the rear surface and escape they establish a TV/m electric field [17, 18], this field can cause the remaining fast electrons to reflect, forming a recirculating (or refluxing) electron population between the surfaces of the target that continues to expand laterally as it recirculates [19, 20]. In thin targets, the proportion of electrons recirculating is a large fraction of the initial beam [16, 21–23] and as they still carry significant energy these electrons are able to generate x-rays as they interact with the bulk of the target [8, 24].

Prior work demonstrates that the effective electron divergence can be varied by changing the interaction conditions. Ovchinnikov *et al* shows that an increased preplasma scale length is a primary driver in electron divergence increase, and a fixed preplasma leads to a constant effective electron divergence over a range of on-target intensities [25, 26]. Measurements of K-alpha signal have shown that effective electron divergence is insensitive to target thickness [26, 27]. Modelling revealed that this was an incomplete picture of the interaction as the initial electron divergence was significantly larger than was measured and collimation of the beam occurred due to field growth which reduced the effective fast electron divergence [16, 28]. Quinn *et al* developed a recirculation model to investigate K-alpha emission in targets with and without the rear surface sheath (controlled via a CH layer on the rear surface), predicting that recirculating electrons could drive a 200 μm K-alpha source from a 20 μm thick Cu target [8].

This paper explores the population of the recirculating electron beam's contribution to the x-ray source via experimental measurements. In this article, we show a dual-source structure in the x-ray signal; (1) a bright narrow core (central source), and (2) a diffuse secondary signal (substrate source) produced by recirculating electrons. It is shown, via analytical modelling, that by tuning the fast electron temperature to the target thickness and material we can minimise the electron recirculation and reduce the contribution from the substrate source whilst increasing the brightness of the central x-ray emission.

2. Experimental Investigation

2.1. Layout

The experiment was conducted using the Vulcan laser [29]. The laser pulse duration was (2.0 ± 0.6) ps, the on-target energy was 80 J providing a peak intensity of $\sim 5 \times 10^{19}$ W cm^{-2} [30, 31]. The targets were copper foils 3 × 7 mm in transverse size and 100 μm thick with the position relative to best (smallest spot diameter) focal position referred to as ΔZ, the laser spot at each defocus position was characterised via a ×20 imaging system with a CCD. Protons accelerated from the rear surface were measured with a Thomson Parabola along the target normal axis. The x-ray source profile was characterised using a penumbral technique similar to the rolled bar shown by Houck and Richardson in 1998 for synchotron emission [32].

The penumbral foil used was a curved sheet of 300 μm tungsten foil, it was set to ∼150 mm radius of curvature to ensure that the transmission length of the x-rays sufficiently attenuates up to 100 keV energies at a small depth (<1 μm) into the foil. The x-rays were detected using Fujifilm SR image plate (IP), with an 18 mm SiO_2 filter between the IP and the interaction. This filters out the low energy x-rays

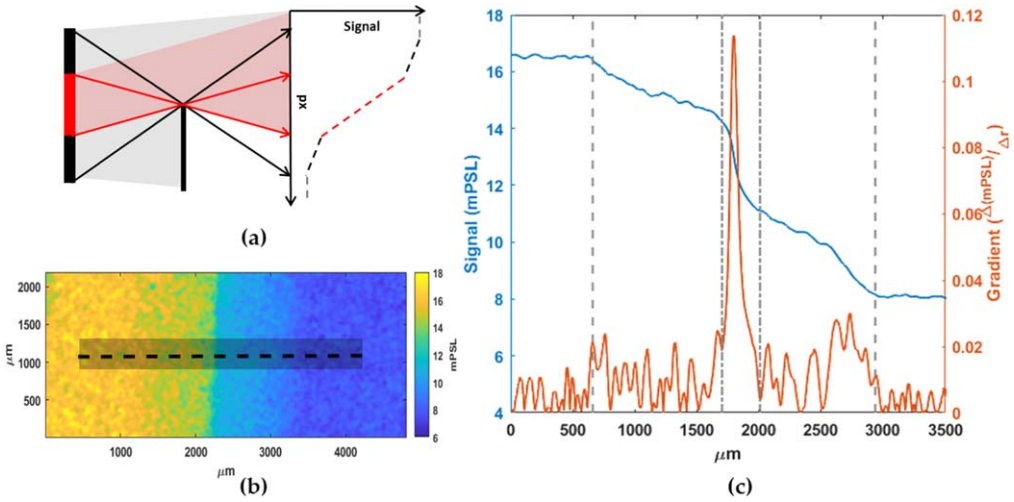

Figure 2. Operation of the penumbral foil, (a) schematic outlining the expected response from a two source x-ray signal, red a bright central source, and grey a larger substrate source (b) is a radiograph of the penumbral foil from a 100 μm thick target at best focus. (c) The lineout and gradient from (b), the dashed lines highlight the two source boundaries, dot–dash for central source, and dashed for the substrate. Lineouts are an average over 250 μm to minimise noise, indicated by the shaded region in (b).

providing a peak absorption at ~ 50 keV. The response curve for the detector, accounting for the SiO_2 filter, is shown in figure 1(b). The penumbral foil was aligned 30^o vertically from the target and set up with a $\times 5.7$ magnification onto the detector plane, with a 0.6 T magnet to remove electron signal from the detector. The total x-ray flux from the target was also measured with secondary IP positioned beneath the penumbral detector on the same plane as the laser. The single foil limits measurements to the horizontal axis of the source; for foil targets under similar laser intensities the source has been demonstrated to be *quasi*-symmetric [33]. With an asymmetric source the imaging quality would be reduced in one axis compared to the other, potentially omitting features that would otherwise be visible.

2.2. Penumbral operation

The penumbral foil creates a near binary transmission object from which the x-ray source characteristics can be determined. When illuminated with a non-point source this will create a transition region in the detected image where the x-ray signal changes gradually. A schematic and example of the penumbral measurement is shown in figure 2 for a 100 μm thick Cu target. The distinct regions of the source are highlighted. Isolating the central source allows the source size and relative flux from both the central electron beam and the recirculating electrons (substrate source) to be retrieved. To do this, we first determine the peak gradient and its full-width-half-maximum. The next point of inversion in the gradient, marked in figure 2(c) by the dot–dash lines, is set as the boundary of the central source and this region is removed from the lineout. This routine is then repeated, this time without the bright contribution from the central source.

The two sets of dashed lines, figure 2(c), highlight the distinct regions in the source—dot–dash for central and dashed for the substrate. Conventional x-ray tube sources have shown a similar double-source structure from penumbral measurements via reconstruction instead of direct measurement [34]. Uncertainty in x-ray source measurements with the penumbral foil are a convolution of both the point spread function—dominated by x-rays scattering through filter materials—and minimum resolution bounds, demonstrated by Fiksel *et al* to be (118 $\pm$ 2) μm for SR IP, due to scattering in the energy deposition and the scanning mechanism [35]. To determine incident photons on each detector, from the measured mPSL, the conversion presented by Bonnet *et al* is used to provide the relative photon numbers per Steradian presented in the paper [36].

2.3. Flux measurements

Figure 3(a) shows the total normalised flux of x-ray emission and number of protons as a function of laser defocus, the number of protons falls with increasing defocus whilst the x-ray signal remains relatively constant. This indicates to a first order approximation that as the laser is defocused, and the on-target laser intensity reduced, there are a similar number of accelerated electrons travelling within the target (creating bremsstrahlung as they travel) yet the number of these electrons reaching the rear surface and contributing to the acceleration of protons has decreased. The measured x-ray signal is consistent with K-alpha measurements modelled by Reich *et al* for copper targets irradiated at similar laser intensities [5, 37]. If we consider each region independently via the penumbral technique outlined above—figure 3(b) we see an increase in x-ray flux from the central source for larger defocus and, more pertinently, the ratio between the central and substrate source shifts significantly in favour of the central source—figure 4(a).

At the maximum defocus tested we see a $\times(10 \pm 2)$ increase in the ratio between the two source components compared to best focus. As the laser intensity is reduced the temperature, $E_h = k_B T_e$, of the fast electron population decreases and the associated attenuation length, $\lambda_{\mathrm{Att.}}(E_h)$, of

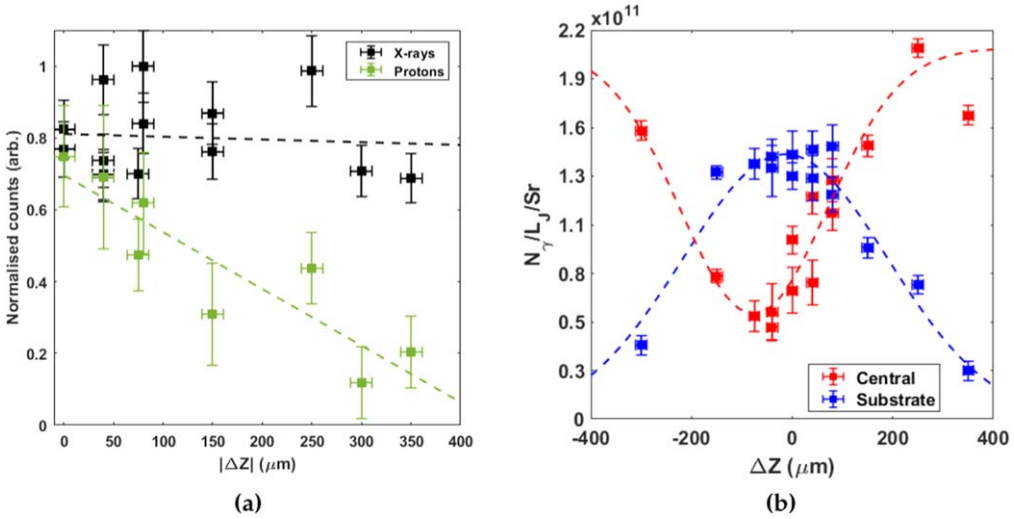

Figure 3. X-ray and proton flux as a function of defocus. (a) Total x-ray flux per laser Joule and number of protons. (b) X-ray flux at 50 keV contributed by each source, central (red) and substrate (blue). Lines of best fit (dashed) are included as a visual aid, linear for (a) and Gaussian for (b).

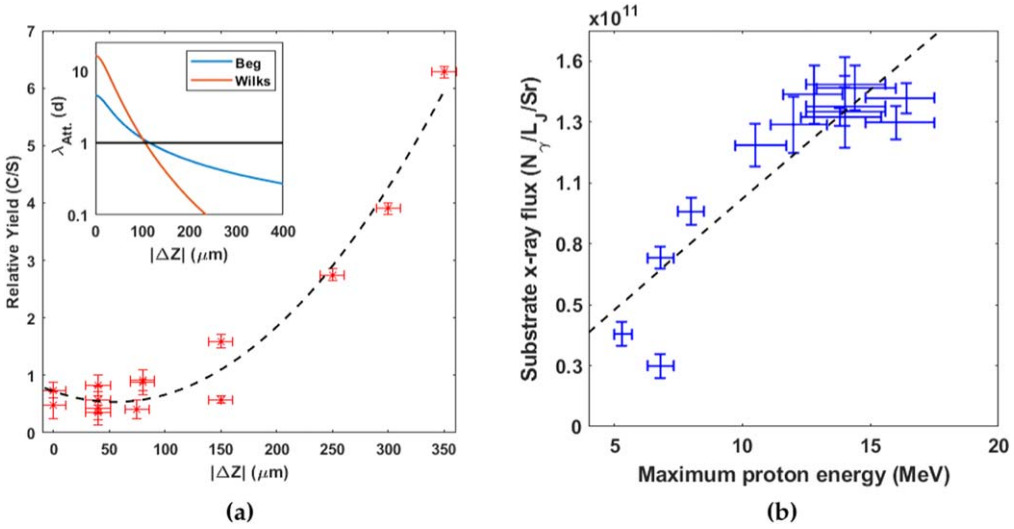

Figure 4. Comparison between the x-ray flux in each region of the x-ray source for varying focus position. (a) Ratio of the central source to the substrate source, more flux is contributed by the central source for increasing defocus. Inset shows the attenuation length, $\lambda_{\mathrm{Att.}}$, normalised to the target thickness, d, for electrons with energy $E = k_B T_e$ in a copper target for Wilks (orange) and Beg (blue) scaling law as a function of defocus position. (b) Substrate x-ray flux as a function of maximum proton energy demonstrating how the sheath influences the recirculating electron current.

the mean electron energy approaches the target thickness in copper. Conversion efficiency, from laser energy to number of fast electrons, has been demonstrated by several groups [38, 39] to scale with intensity. A reduced temperature spectra could have more electrons populating it though, even when factoring in the reduced laser conversion, as the temperature reduces faster than the absorption with intensity. The inset of figure 4(a) shows the attenuation length in copper for both the scaling arising from Wilks *et al* [40] and Beg *et al* [2]. For each scaling law the attenuation length of the expected fast electron temperature with copper approaches the target thickness at $\sim$150 μm defocus. This is the same defocus that we begin to see the central source dominate in flux contribution. This implies that the central source is dominated by electrons on their first pass of the target, and that, by contrast, the substrate source must be generated by either a subset of highly-divergent fast electrons or electrons that are recirculating through the target. The latter is known to be a significant fraction of the accelerated electron population [19, 20, 24] and therefore will be considered here. The recirculating fast electron population is dependent on the sheath field established on the target rear surface which stops electrons escaping on the first pass of the target. In figure 4(b) the maximum proton energy and the x-ray flux contribution of the substrate source is compared, demonstrating a linear relationship between the two.

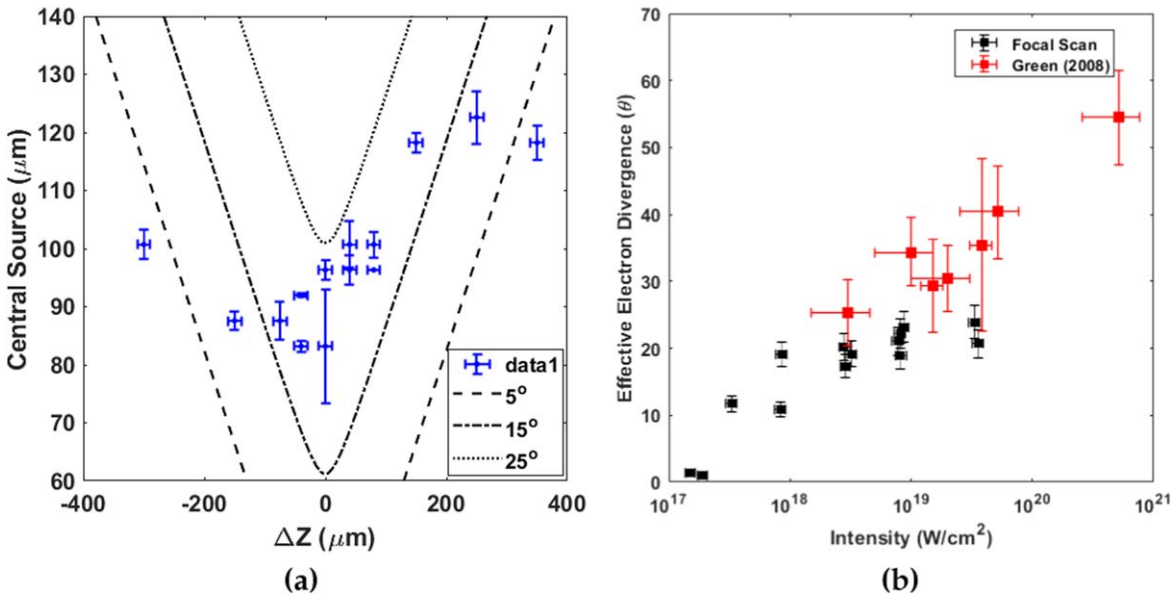

Figure 5. Central x-ray source size and electron divergence as a function of defocus. (a) Central source size as measured (blue), with the expected size from a simple geometric expansion for different electron divergences also shown (black dashed lines). (b) Electron divergence as a function of on target intensity. Measurements from this experiment (black) extend the trend seen in numerous experiments collated by Green *et al* (red), references of each in [26]. Reprinted with permission from [26], Copyright (2008) by the American Physical Society.

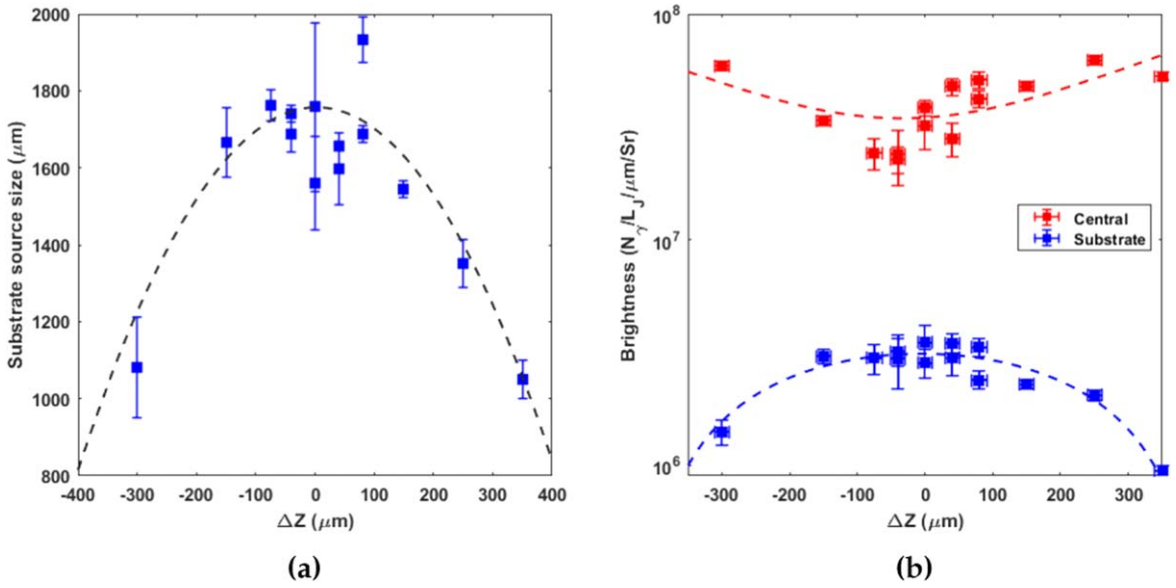

Figure 6. (a) Source size for substrate x-ray source as a function of defocus position. (b) Brightness of the two sources as a function of defocus position showing an increase in central brightness as the laser is defocused.

2.4. Spatial x-ray measurements

The results above suggest a mechanism to improve x-ray radiography by reducing the contribution by the larger substrate source. Figures 5(a)–6(a) are plots of the lateral size of both the central and substrate source as a function of defocus position. The trend with defocus (ΔZ) seen in the central source size cannot be approximated by a single electron divergence, as demonstrated in figure 5(a). However, the divergence of the electrons through the target can be inferred from the central measurement and laser spot diameter. We find good agreement with the divergence measurements made by Green *et al* [26] over the tested intensity range, figure 5(b). It should be noted that the ~50 keV x-rays measured by the diagnostic will have reduced divergence compared to the isotropic K-alpha signal measured by Green *et al* due to the bremsstrahlung generation mechanism conserving momentum from the incident relativistic electron [41]. From GEANT4 simulations [42] the electrons responsible for generating the majority of the detected x-ray flux is ~1–2 MeV for the expected laser intensity.

The central source increases as the laser is defocused, from an optimum of ~84 to >120 μm at largest defocus whereas the substrate source decreases from ~1.8 mm at best

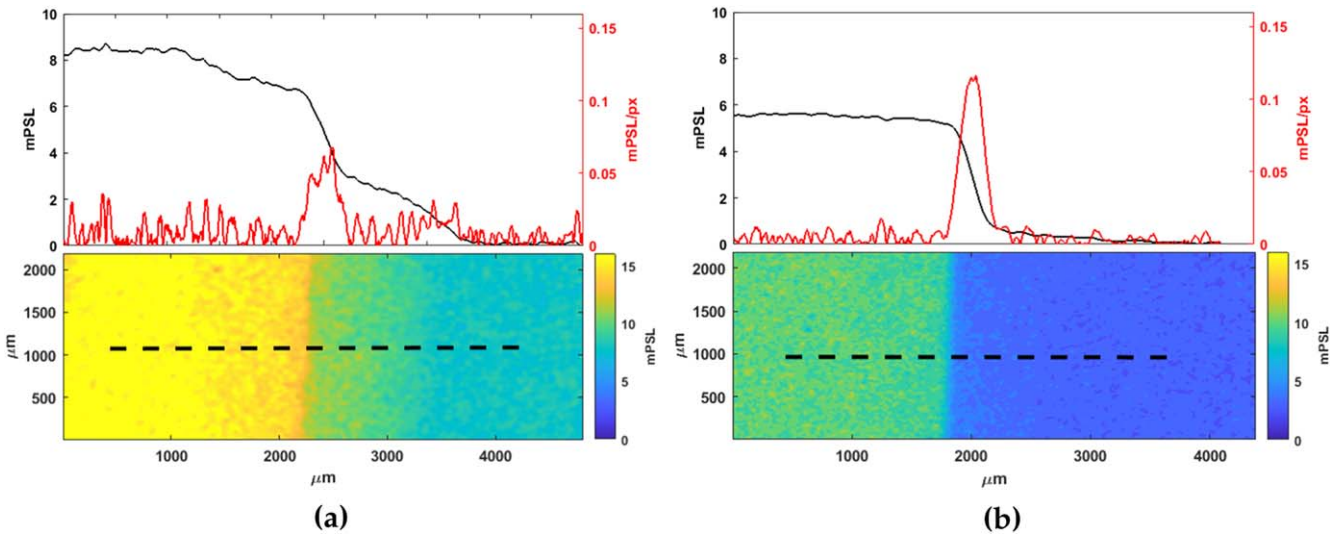

Figure 7. Comparison of varying defocus in radiographs, (a) target at best focus, (b) target at $-300\ \mu$m defocus. The significant image contrast improvement by reducing, or removing, the secondary source is clear.

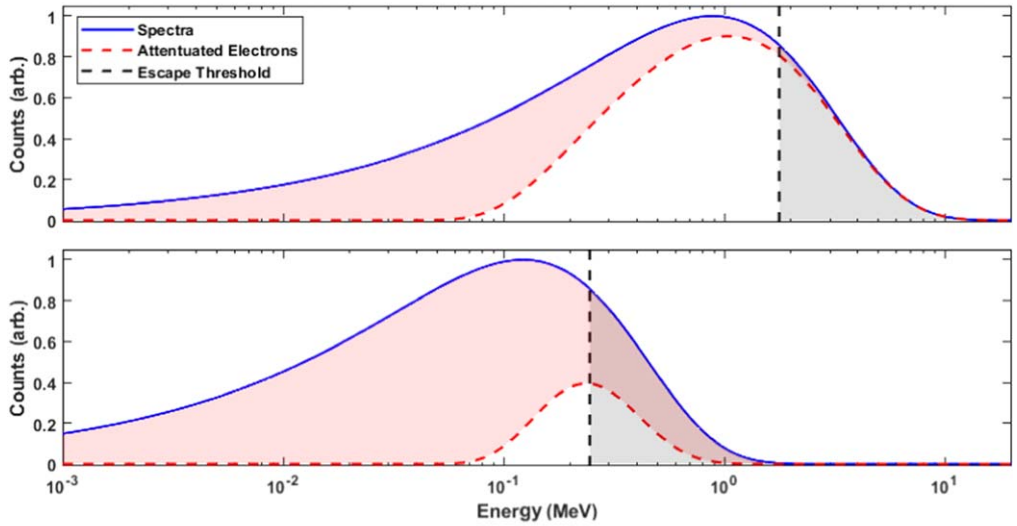

Figure 8. Maxwellian distribution for electrons with temperature $k_B T_e$ at two different laser intensities, top for 1×10^{20} W cm^{-2} and bottom for 4×10^{18} W cm^{-2}, this correlates to the laser at best focus and 150 μm defocus. The red dashed line indicates electron transmission through the target, black dashed line is the escape energy cut-off. The population of electrons between these two lines contributes to the substrate source (unshaded), the other two (red—collisional, gray—escaping) can only contribute to the central source.

focus to $\simeq$1 mm at large defocus. A lineout of the penumbral edge at best focus and largest defocus is presented in figure 7. Whilst the increase in the central source can be explained by the increasing laser focal spot and reduced electron divergence the decreasing size of the substrate source and the reduction in the x-ray flux shown in figure 4(a) is indicative of a lower total number of recirculating electrons.

Magnified spatial resolution of a radiograph is dependent on the detector resolution and the size of the source emission area. As such, decreasing the size and flux contribution of the substrate source is beneficial to radiography as it removes the larger blurring factor on the image. The increase in central source size, however, is overcome by the increase in flux driving a brighter central source, shown in figure 6(b).

2.5. Spatial contrast improvement

The spatial profile of the x-ray source demonstrates a two-source structure, a narrow central channel and a broad substrate source. The increased contrast between the central and substrate source provides greater spatial contrast of the x-ray emission and the reduction of the secondary source removes the majority of the background signal. When the ratio between these two sources is at its greatest (i.e 300 μm defocus from the experimental scan) the image quality is at its greatest. An example of this can be seen in the radiographs in figure 7.

Whilst the radiograph of the penumbral edge can be considered as a simplified—almost ideal—example, the

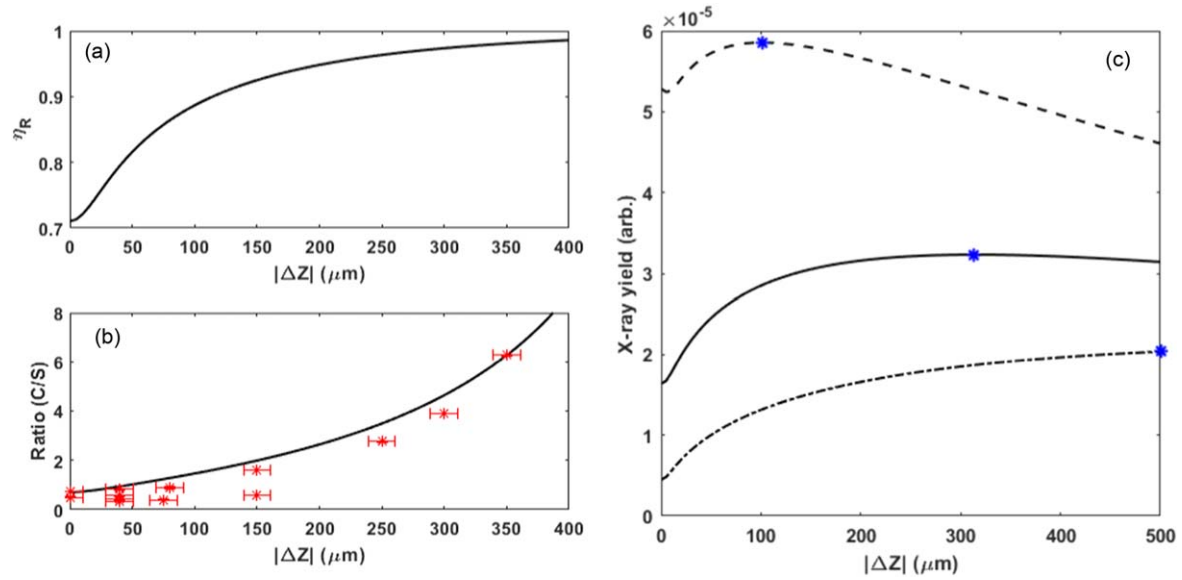

Figure 9. Results from the analytical model. (a) Population of electrons that contribute only to the central source, equation (3) as a function of defocus (b) is the ratio calculated as $\eta_R/2(1-\eta_R)$ with the experimental data. (c) Is the central x-ray flux calculated for various targets: copper—solid, tantalum—dashed, and aluminium—dot–dash, the peak flux shown with a blue asterisk.

increase in contrast is clear. Objects with features smaller than the substrate source could be blurred by its contribution.

3. Discussion

Analytically we can begin to understand the emergence of this effect for targets of given thickness by considering how to optimise the x-ray flux created on the first pass of the target (i.e. those fast electrons that only travel in the central channel). We know from scaling laws that the intensity and fast electron relationship scales as, $I^a \propto k_B T_e$, where $k_B T_e$ is the hot electron temperature and a varies from 0.33 [2] to 0.5 [40]. The sheath evolves via plasma expansion. Mora [43] presents a 1D isothermal plasma expansion model that can be used in calculations of the sheath dynamics. The peak electric field E_{sheath} scales as:

$$E_{\text{sheath}} \propto (n_e k_B T_e)^{0.5}, \tag{1}$$

where n_e is the electron density. If the separation between the target surface and the peak of the sheath is λ_D then the energy of electrons able to escape the target can be approximated to:

$$U_{\text{esc}} \simeq E_{\text{sheath}} \lambda_D \simeq k_B T_e. \tag{2}$$

Electrons with more than this energy typically can escape the target on the first pass and as such only contribute to the central source of x-rays. The other sub-population to consider is the low energy electrons, those that would typically lose their energy through collisions with the bulk target in a single pass. This limits low energy electrons from reaching the rear surface based on the target material and thickness, with the transmission function, Γ, defined as: $\Gamma(E_h, \rho, l) = \exp(-l\rho\sigma(E_h))$, where $\sigma(E_h)$ is the attenuation cross section for an electron of energy E_h, ρ and l are the target density and thickness respectively. The remaining electrons contribute to the substrate source and blur the final image. The ratio of electrons that can only contribute to the central source and those that recirculate and contribute to the substrate source can be expressed as, η_R:

$$\eta_R = \frac{N_c + N_e}{N_h} = \frac{\int_0^\infty (1-\Gamma) f(E_h) \mathrm{d}E_h + \int_{k_B T_e}^\infty f(E_h) \mathrm{d}E_h}{\int_0^\infty f(E_h) \mathrm{d}E_h}, \tag{3}$$

where N_e, N_c, and N_h are the populations of escaping electrons, electrons lost through collisions in the target, and the total number of accelerated electrons respectively.

The distribution is a Maxwellian of the form $f(E_h) = A\sqrt{\frac{4E_h}{\pi (k_B T_e)^3}} \exp\left(-\frac{E_h}{k_B T_e}\right)$, where A is the conversion efficiency calculated from the equation presented in Davies [44]. Figure 8 shows these for a typical spectra for a high intensity laser. The difference between the total number accelerated and those that escape or collide through the target are the recirculating electrons. In order to maximise the central source of x-rays the collisional and escaping electron populations need to be significantly greater in number than the recirculating electrons. This model is calculated from intensity and does not implicitly include temporal or energy considerations that are known to alter the sheath development [43, 45–47]. We would expect a similar optimum to exist when varying either energy or pulse duration, when the sheath field and electron attenuation result in a lower recirculating population. This model gives us a method to optimise the electron temperature to the target thickness, maximising the central source distribution and therefore the final image quality. To correlate this with the experimental work the intensity was determined by 80 J in a spot defined by $\sqrt{(2.44\lambda F_\#)^2 + \left(\frac{\Delta Z}{F_\#}\right)^2}$, where λ is the wavelength of the laser, $F_\#$ is the F-number of the final focussing optic of the laser, with a 2 ps pulse duration. The results and the expected

ratio between the two sources is shown in the lower plot of figure 9(a) with the results from the experimental campaign also plotted. The ratio of x-ray yields is calculated from the electron populations by the ESTAR radiative stopping power tables [48] with the recirculating population contributing on every other pass of the target to account for the directionality of the emission.

By changing the model parameters to include different target conditions we can probe the optimum intensity conditions for these targets. The dashed lines in figure 9(b) show the curves for tantalum (dashed) and aluminium (dot–dash) targets at 100 μm thickness peaking at different intensity regions compared to the copper target. The model peaks at $\sim$300 μm defocus for copper targets, agreeing with the experimental data presented in figure 3(a).

4. Conclusion

The x-ray spatial profile from a high intensity laser-solid interaction results in a dual-source structure. The central channel dominated by fast electrons on their first pass through the target and a larger substrate source from recirculating electrons spreading laterally during their multiple passes through the target. Experimental results demonstrate a $\times(10 \pm 2)$ increase in the ratio of the central source to the substrate source, suggesting a way to increase the quality of x-ray radiographs by optimising this ratio and the flux. Through analytical modelling we are able to probe this relationship as a ratio between escaping, attenuated, and recirculating electrons and present optimum laser intensities for varying target parameters. The model provides good agreement with the experimental data, in terms of both the ratio between central and substrate x-ray flux and the total central x-ray flux produced.

Acknowledgments

This work was supported by the Newton Fund for STFC UK-China Laser driven Ion and THz, NSFC grant 11520101003, EPSRC grants EP/K022415/1 and EP/R006202/1, and the STFC IPS grant ST/P000177/1. We also acknowledge the use of the EPOCH PIC code (developed under EPSRC grant EP/G054940/1) and the computing resources provided by STFC Scientific Computing Department's SCARF cluster. Data associated with research published in this paper is accessible at: https://doi.org/10.15129/b5afec6a-f3fa-463b-b0a7-436b999229c5.

ORCID iDs

C D Armstrong https://orcid.org/0000-0003-2083-8487
N C Woolsey https://orcid.org/0000-0002-2444-9027
P McKenna https://orcid.org/0000-0001-8061-7091

References

[1] Bell A R, Davies J R, Guerin S and Ruhl H 1997 *Plasma Phys. Control. Fusion* **39** 653–9
[2] Beg F N, Bell A R, Dangor A E, Danson C N, Fews A P, Glinsky M E, Hammel B A, Lee P, Norreys P A and Tatarakis M 1997 *Phys. Plasmas* **4** 447–57
[3] Gibbon P 2004 *Short pulse laser interactions with matter* (London: Imperial College Press)
[4] Brenner C M *et al* 2015 *Plasma Phys. Control. Fusion* **58** 014039
[5] Reich C, Gibbon P, Uschmann I and Forster E 2000 *Phys. Rev. Lett.* **84** 4846–9
[6] Perry M D, Sefcik J A, Cowan T, Hatchett S, Hunt A, Moran M, Pennington D, Snavely R and Wilks S C 1999 *Rev. Sci. Instrum.* **70** 265
[7] Edwards R D *et al* 2002 *Appl. Phys. Lett.* **80** 2129–31
[8] Quinn M N *et al* 2011 *Plasma Phys. Control. Fusion* **53** 025007
[9] Chen C D *et al* 2008 *Rev. Sci. Instrum.* **79** 130–3
[10] Meadowcroft A L and Edwards R D 2012 *IEEE Trans. Plasma Sci.* **40** 1992–2001
[11] Rusby D, Gray R, Butler N, Dance R, Scott G, Bagnoud V, Zielbauer B, McKenna P and Neely D 2018 *EPJ Web Conf.* **167** 02001
[12] O'Neill D M, Lewis C L S, Neely D, Davidson S J, Rose S J and Lee R W 1991 *Phys. Rev.* A **44** 2641
[13] Moore C I, Knauer J P and Meyerhofer D D 1995 *Phys. Rev. Lett.* **74** 2439–42
[14] Wei M S, Solodov A A, Pasley J, Stephens R B, Welch D R and Beg F N 2008 *Phys. Plasmas* **15** 0–7
[15] Scott R H H *et al* 2012 *Phys. Rev. Lett.* **109** 1–5
[16] Yuan X H *et al* 2010 *New J. Phys.* **12** 063018
[17] Hegelich M *et al* 2002 *Phys. Rev. Lett.* **89** 085002/1
[18] Poyé A *et al* 2015 *Phys. Rev.* E **91** 043106
[19] Chen H and Wilks S C 2005 *Laser Part. Beams* **23** 411–6
[20] Mackinnon A J, Sentoku Y, Patel P K, Price D W, Hatchett S, Key M H, Andersen C, Snavely R and Freeman R R 2002 *Phys. Rev. Lett.* **88** 2150061
[21] Sentoku Y, Cowan T E, Kemp A and Ruhl H 2003 *Phys. Plasmas* **10** 2009–15
[22] Myatt J, Theobald W, Delettrez J A, Stoeckl C, Storm M, Sangster T C, Maximov A V and Short R W 2007 *Phys. Plasmas* **14** 056301
[23] Neely D, Foster P, Robinson A, Lindau F, Lundh O, Persson A, Wahlstrom C G and McKenna P 2006 *Appl. Phys. Lett.* **89** 87–90
[24] Fiorini F, Neely D, Clarke R and Green S 2014 *Laser Part. Beams* **32** 233–41
[25] Ovchinnikov V M, Schumacher D W, McMahon M, Chowdhury E A, Chen C D, Morace A and Freeman R R 2013 *Phys. Rev. Lett.* **110** 1–4
[26] Green J S *et al* 2008 *Phys. Rev. Lett.* **100** 015003
[27] Lancaster K L *et al* 2007 *Phys. Rev. Lett.* **98** 125002
[28] Coury M *et al* 2013 *Phys. Plasmas* **20** 043104
[29] Musgrave I, Galimberti M, Boyle A, Hernandez-Gomez C, Kidd A, Parry B, Pepler D, Winstone T and Collier J 2015 *High Power Laser Sci. Eng.* **3** e26
[30] Bradford P *et al* 2018 *High Power Laser Sci. Eng.* **6** 8
[31] Liu H *et al* 2018 *Rev. Sci. Instrum.* **89** 083302
[32] Houck T L and Richardson R A 1998 *Roll bar x-ray spot size measurement technique* No. UCRL-JC–130427 Lawrence Livermore National Laboratory pp 908–10
[33] Courtois C *et al* 2009 *Phys. Plasmas* **16** 013105
[34] Kueh A, Warnett J M, Gibbons G J, Brettschneider J, Nichols T E, Williams M A and Kendall W S 2016 *J. X-Ray Sci. Technol.* **24** 583–97

[35] Fiksel G, Marshall F J, Mileham C and Stoeckl C 2012 *Rev. Sci. Instrum.* **83** 88–91
[36] Bonnet T, Comet M, Denis-Petit D, Gobet F, Hannachi F, Tarisien M, Versteegen M and Aleonard M M 2013 *Rev. Sci. Instrum.* **84** 103510
[37] Reich C, Uschmann I, Ewald F, Düsterer S, Lübcke A, Schwoerer H, Sauerbrey R, Förster E and Gibbon P 2003 *Phys. Rev.* E **68** 056408
[38] Ping Y *et al* 2008 *Phys. Rev. Lett.* **100** 6–9
[39] Gray R J *et al* 2018 *New J. Phys.* **20** 033021
[40] Wilks S C, Langdon A B, Cowan T E, Roth M, Singh M, Hatchett S, Key M H, Pennington D, MacKinnon A and Snavely R A 2001 *Phys. Plasmas* **8** 542–9
[41] Lawson J D 1950 *Proc. Phys. Soc.* A **63** 653–60
[42] Agostinelli S *et al* 2003 *Nucl. Instrum. Methods Phys. Res.* A **506** 250–303
[43] Mora P 2003 *Phys. Rev. Lett.* **90** 4
[44] Davies J R 2009 *Plasma Phys. Control. Fusion* **51** 014006
[45] Oishi Y *et al* 2005 *Phys. Plasmas* **12** 1–5
[46] Fuchs J *et al* 2006 *Nat. Phys.* **2** 48–54
[47] Brenner C M *et al* 2011 *Laser Part. Beams* **29** 345–51
[48] Berger M J, Hubbell J H, Seltzer S M, Chang J, Coursey J S, Sukumar R, Zucker D S and Olsen K 1998 Stopping-Power and Range tables for Electrons, Protons, and Helium Ions https://doi.org/10.18434/T48G6X
[49] Yuan X H *et al* 2011 *Nucl. Instrum. Methods Phys. Res.* A **653** 145–9